Research Article | Vol. 29, No. 11 / 24 May 2021 / Optics Express 16396
Optics EXPRESS

Metamaterial perfect absorber simulations for intensifying the thermal gradient across a thermoelectric device

SHOHEI KATSUMATA,[1] TAKUO TANAKA,[2,3,4,5] AND WAKANA KUBO[1,*]

[1]Division of Advanced Electrical and Electronics Engineering, Tokyo University of Agriculture and Technology, 2-24-16 Naka-cho, Koganei-shi, Tokyo 184-8588, Japan
[2]Metmaterial Laboratory, RIKEN Cluster for Pioneering Research, 2-1 Hirosawa, Wako, Saitama 351-0198, Japan
[3]Department of Physics, Faculty of Science, Gakushuin University, 1-5-1 Mejiro, Toshima-ku, Tokyo 171-8588, Japan
[4]Innovative Photon Manipulation Research Team, RIKEN Center for Advanced Photonics, 2-1 Hirosawa, Wako, Saitama 351-0198, Japan
[5]Institute of Post-LED Photonics, Tokushima University, 2-1 Mishima, Minami-Jyosanjima, Tokushima 770-8560, Japan
*w-kubo@cc.tuat.ac.jp

Abstract: The thermal gradient across a thermoelectric device is the key to convert heat energy into electricity. Here, we propose a metamaterial perfect absorber (MPA) that increases the thermal gradient across a thermoelectric device by local heat generation through absorbing thermal radiation emitted from an infinite-size blackbody radiator. The MPA, when attached on top of a bismuth telluride thermoelectric device, generates local heat that propagates to the device, resulting in an additional thermal gradient. The amount of local heat generated at the MPA and the output power of the thermoelectric device loaded with the MPA are examined through numerical calculations.

1. Introduction

Thermoelectric energy conversion is a technology based on direct conversion of heat energy into electricity. It is expected to be a promising tool for more efficient fuel usage and energy saving [1]. Since a thermal gradient across a thermoelectric device induces a potential difference between the hot and cold sides of the device, a technology that increases the thermal gradient is the key for efficient power generation. Several attempts have been made to increase the thermal gradient in thermoelectric devices. Vertical geometric configuration of the thermoelectric device to the surface of a heater is a promising strategy to enlarge the thermal gradient across the device. In fact, the performance of a thermoelectric device is affected by geometrical factors, such as the device configurations and morphology of its thermoelectric legs. Pyramid-shaped legs of bismuth telluride (Bi_2Te_3) can provide better power density than rectangular shaped legs since the pyramid shape lowers the thermal conductance, leading to a larger thermal gradient [2]. Nevertheless, the power generation efficiencies of Bi_2Te_3-based thermoelectric devices remain at ~10%, indicating that further improvements are required. Hence, developing novel thermoelectric materials and ideas to enlarge the thermal gradient is necessary to expand the practical applications of thermoelectric devices.

To increase the thermal gradient across a thermoelectric device, we utilized localized surface plasmon resonance as the heat source. Plasmonic structures absorb electromagnetic waves, resulting in plasmonic local heat generation as a consequence of plasmon loss [3,4]. Previously, we demonstrated photodetection based on plasmonic photo-thermoelectric conversion that

#418814 https://doi.org/10.1364/OE.418814
Journal © 2021 Received 29 Jan 2021; revised 13 Apr 2021; accepted 22 Apr 2021; published 12 May 2021

Optics EXPRESS

converts light energy into electricity by plasmonic local heating and thermoelectric conversion. The plasmonic local heating was utilized to induce thermoelectric conversion by creating a thermal gradient across the thermoelectric film under light illumination [5,6]. Light illumination on the plasmonic atoms excites the localized surface plasmons and generates plasmonic local heating. This plasmonic local heating will propagate to the surrounding media and create a thermal gradient, resulting in a potential difference between the edges of the thermoelectric film. The amount of plasmonic local heat should not be underestimated as it is a reliable resource for energy conversion. In fact, several studies have demonstrated the importance of local heating and proposed applications in photodetection [7], thermal therapy [8,9], nanowire growth [10], and photocatalysis [11]. Since the material properties and configurations of the plasmonic structure determine their resonance wavelength region, an appropriate selection of material and configuration enables us to realize a photodetector driven in the visible [12,13] and infrared (IR) regions [14,15]. Thus, well-designed plasmonic atoms can convert electromagnetic radiation into electricity by local heating; this concept can be used to improve power conversion efficiency of thermoelectric devices.

In this study, we propose the attachment of a metamaterial perfect absorber (MPA) on the surface of a Bi_2Te_3 thermoelectric device, put in a 500.15 K-temperature environment, to realize a thermoelectric device driven by the absorption of thermal radiation. Notably, Bi_2Te_3 is the best thermoelectric material for a temperature range below 500 K [16,17]. A MPA consists of two distinct metal nanostructures sandwiching a thin dielectric layer as a spacer [18,19]. The MPA is known to absorb any incident light owing to its magnetic resonance and can convert absorbed light into local heat more effectively than other plasmonic atoms. This means that the MPA with a resonance band in the IR region absorbs thermal radiation emitted from a heat source, resulting in generation of local heat. This local heating will create an additional thermal gradient across the Bi_2Te_3 thermoelectric device as a result of local heat propagation, leading to better device performance in thermoelectric conversion.

To realize a thermoelectric device that can harvest low-temperature waste heat, we designed a MPA that interacts with radiation heat at 500.15 K (227.0 °C) and placed it on a conventional thermoelectric material. We numerically calculated the amount of local heat generated at the MPA that absorbs thermal radiation at 500.15 K using the finite element method and thermoelectric simulations.

Finally, we estimated the output power per unit area of the thermoelectric device loaded with the MPA. To the best of our knowledge, this is the first proposal to utilize the local heating of the metamaterial generated by the absorption of thermal radiation to enhance the thermoelectric device performance. Furthermore, it is important to visualize the power generation efficiency of the device through numerical calculations. This will pave the way for the realization of a practical device. We selected 500.15 K as the temperature of the heat source because most of the unrecovered waste heat (60% of the total waste heat) is at temperatures below 500 K. However, our strategy can be adapted to other temperatures by tuning the structure of the MPA [20,21].

2. Numerical experiments

Figure 1 shows the schematics of a single unit of the Bi_2Te_3 thermoelectric device loaded with the MPA on its surface (Fig. 1(a)) and the whole configuration consisting of multiple units (Fig. 1(b)). The area and thickness of the Bi_2Te_3 thermoelectric device are 1 cm^2 and 1 mm, respectively. The MPA was designed to have an absorption peak at 6.0 μm, consistent with the blackbody radiation peak at 500.15 K. The MPA consists of an Ag layer (bottom) and disks (top) that sandwich a thin dielectric layer of calcium fluoride (CaF_2) that does not strongly absorb in the IR region. The Ag layer at the bottom has a thickness of 100 nm, and acts as a mirror for the absorber and as a thermal conductor between the MPA and the Bi_2Te_3. In addition, the Ag

Optics EXPRESS

bottom layer functions as an electrode at the hot side of the thermoelectric device. The Bi_2Te_3 thermoelectric device has a Cu electrode at the cold side to extract electricity (Fig. 1(a)).

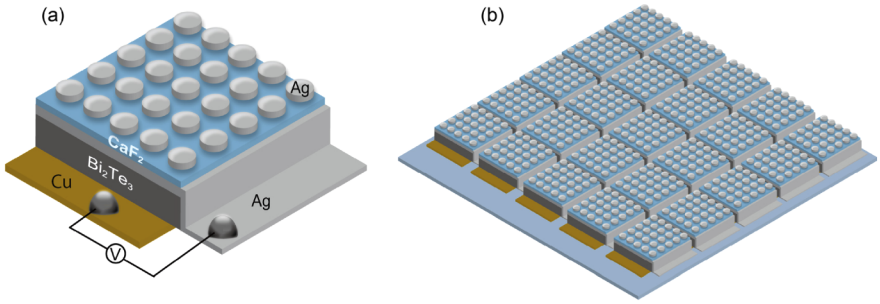

Fig. 1. Schematics of the Bi_2Te_3 thermoelectric device with metamaterial perfect absorber arrays: (a) single unit device and (b) full device consisting of integrated units.

Since the diameter and periodicity of the Ag disks, and the thickness of the CaF_2 layer significantly affect the absorption band of the MPA, we optimized these parameters first. Numerical simulations of the reflectance of the MPA, the amount of local heat generated at the MPA, and the output power generated between the Cu and Ag electrodes were performed using the COMSOL Multiphysics finite element solver. Such calculations were performed assuming that the MPA faces the infinite-size blackbody radiator at 500.15 K. This meant that the Cu electrode at the bottom of the Bi_2Te_3 thermoelectric device was 500.15 K. Numerical simulations of the local heat were carried out at 500.15 K; the whole device was at thermal equilibrium. The size of the blackbody was sufficiently larger than that of the thermoelectric device. The blackbody heat source emits a thermal radiation spectrum according to Planck's law. The MPA absorbs a part of the thermal radiation emitted by the blackbody heat source and generates local heating as a consequence of plasmon loss. The local heat propagates to the Bi_2Te_3 thermoelectric device, resulting in an increase in the temperature difference between the hot and the cold ends of the device, and subsequently an increase in the output power.

3. Results and discussions

3.1. Optimization of MPA

Figure 2(a) shows the spectral dependences of the reflectivity of MPA on structural parameters. The periodicity of the Ag disk and the thickness of the CaF_2 layer were fixed at 2.0 μm and 60 nm, respectively, for this optimization. Areas in blue (Fig. 2(a)) indicate lower reflectivity, corresponding to strong absorption induced by the magnetic resonance of the MPA. The area of the lowest reflectivity shifts to longer wavelengths as the diameter of the Ag disk increases. The 1.75-μm-diameter Ag disk shows a reflectivity peak at 6.08 μm; this is close to the blackbody radiation peak at 500.15 K. Hence, we employed the 1.75-μm-diameter Ag disk for further optimizations.

Figure 2(b) shows the reflectivity dependence of the Ag disk periodicity of the MPA on the wavelength. Here, we set the CaF_2 layer thickness at 60 nm. Interestingly, the wavelength of the lowest reflectivity did not change with the periodicity of the Ag disk. On the contrary, the full width at half maximum of the reflectivity peak widened as the Ag disk periodicity narrowed. We utilized Ag disk with periodicity of 2.0 μm for further optimizations.

Figure 2(c) shows the reflectivity dependence of the CaF_2 layer thickness of the MPA on the wavelength. The reflectivity peak wavelengths of the MPA with a CaF_2 layer thicker than 40 nm were almost constant, while those of the MPA with a CaF_2 layer thinner than 40 nm shifted to the longer wavelength. The MPA with a CaF_2 layer thickness in the range of 50–80 nm showed the

Optics EXPRESS

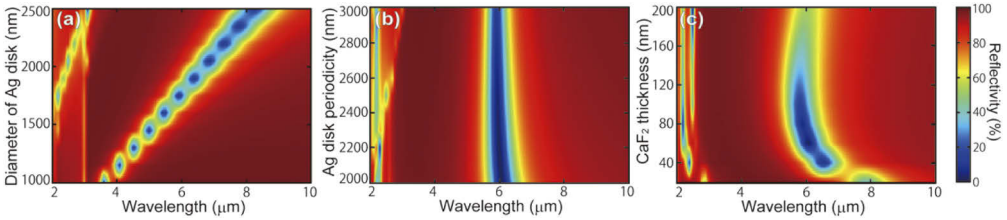

Fig. 2. Dependences of the reflectivity on the structural parameters of metamaterial perfect absorber. Dependence of (a) Ag disk diameter, (b) Ag disk periodicity at a disk diameter of 1.75 μm, and (c) CaF_2 layer thickness as a function of wavelength.

lowest reflectivity of less than 20%. We speculate that the slight peak shift observed in Fig. 2(c) is caused by the near-field coupling between the Ag disk and film, which is determined by the thickness of the CaF_2 layer. It affects the restoring force in the collective oscillations of the free carriers in the Ag disk and film as reported [22]. From these optimizations, MPAs with Ag disk diameters of 1.75-μm, 2-μm-periodicity, and a CaF_2 layer of 60-nm-thickness were fixed for the subsequent investigations. Currently, we have focused on these three parameters to optimize the MPA structure since they are critical for determining the resonance properties of the MPA. However, the thickness dependence of the Ag disk and the Ag layer should be investigated in the future for further optimization.

Figure 3 shows the reflection spectrum of the MPA with 1.75-μm-diameter and 2-μm-periodicity of the Ag disks, and a 60-nm-thick CaF_2 layer. It also shows the blackbody radiation spectrum at 500.15 K. The MPA showed a strong reflection peak at 6.08 μm, indicating that the MPA absorbs a part of the thermal radiation emitted from the infinite-size blackbody radiator at 500.15 K. The strong absorption at 6.08 μm is attributed to the magnetic resonance mode of the MPA, as discussed later in Section 3.2. The strong peak at 2.24 μm is a higher mode of the peak observed at 6.08 μm. The energy absorbed by the MPA will be converted into plasmonic local heat as a consequence of absorption loss, leading to its radial propagation [4,23–25]. Although the Bi_2Te_3 thermoelectric device loaded with the MPAs is faced to the infinite-size blackbody radiator at 500.15 K, most of the local heat is expected to propagate to the surface of the Bi_2Te_3 thermoelectric device via the Ag film, owing to the higher thermal conductivity of Ag. This heat propagation results in an additional thermal gradient across the Bi_2Te_3 thermoelectric device. To estimate the additional output power induced by the MPA, we calculated the amount of local heat generated at the MPA and the output power of the Bi_2Te_3 thermoelectric device.

The reflection spectrum of the Bi_2Te_3 thermoelectric film with a 100 nm-thick-Ag electrode on its top surface was considered as a reference device (Fig. 3) and examined. The calculated reflectivity shown in a broken line was approximately 98% at 6 μm, indicating that the 100 nm-thick-Ag electrode on the Bi_2Te_3 film does not absorb thermal radiation at all.

3.2. *Heat generation of MPA*

We numerically calculated the amount of local heat generated at the MPA using the COMSOL software with RF and heat transfer modules. The RF module was used for the optical calculations of the MPA, and the heat transfer module was used to calculate the local heat generated at the MPA and the thermoelectric simulations. The calculation model involves a single MPA structure surrounded by heat flux layers that permit heat flow from the inside to the outside of the unit. Perfect matching layers were located on the top and bottom of the unit. Plasmonic local heating occurs due to the Joule effects; thus, the heat power density $Q(\mathbf{r})$ can be calculated using Eq. (1) [26],

$$Q(\boldsymbol{r}) = \frac{\omega}{2} Im(\varepsilon(\omega))\varepsilon_0 |\mathbf{E}(\mathbf{r})|^2, \tag{1}$$

Optics EXPRESS

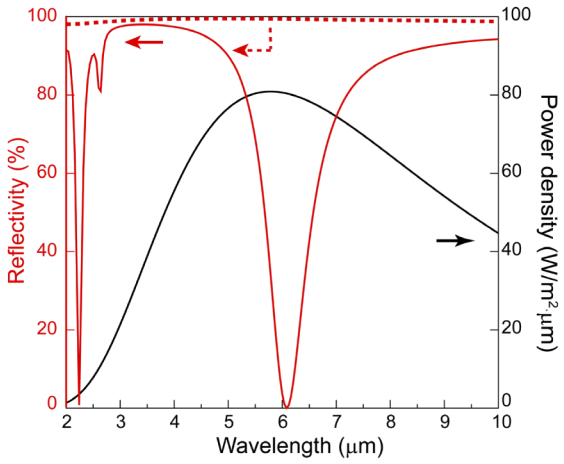

Fig. 3. Reflection spectrum of the metamaterial perfect absorber with 1.75-μm-diameter and 2-μm-periodicity of the Ag disks and a 60-nm-thick CaF_2 layer attached on the Bi_2Te_3 thermoelectric device (red curve), the bare Bi_2Te_3 film with a top Ag electrode (red dashed curve) as a control device, and blackbody radiation spectrum at 500.15 K (black curve).

where $\varepsilon(\omega)$ is the relative permittivity of the material, ε_0 is the vacuum permittivity, *Im* indicates the imaginary part, and $|\mathbf{E}(\mathbf{r})|^2$ is the intensity of the electric field. Figure 4 shows the electric and magnetic field distributions of the MPA calculated at a wavelength of 6.08 μm. Strong electric field confinements were observed at the edges of the Ag disk (Fig. 4(a)), indicating that these edges are the main sites of plasmonic local heating. Strong magnetic field confinement was observed in the CaF_2 layer (Fig. 4(b)), indicating that the strong IR absorption is attributed to this magnetic resonance mode [22,27–29]. In fact, the MPA exhibited an absorbance of 93% at the peak wavelength (6.08 μm in Fig. 3).

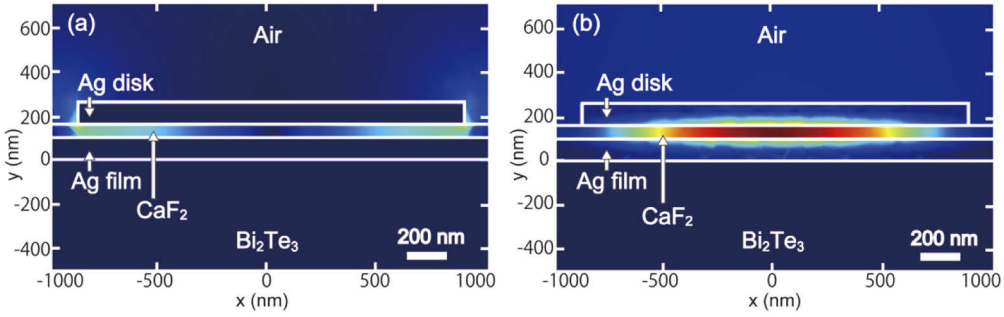

Fig. 4. (a) Electric and (b) magnetic field distributions of the metamaterial perfect absorber with 1.75-μm-diameter and 2-μm-periodicity Ag disks and a 60-nm-thick CaF_2 layer attached on a Bi_2Te_3 thermoelectric device, calculated at a wavelength of 6.08 μm.

Heat transfer in a system can be described by the usual heat transfer and energy conservation equations [30,31],

$$\rho(\mathbf{r})c(\mathbf{r})\frac{\delta T(\mathbf{r})}{\delta t} = \nabla\kappa(\mathbf{r})\nabla T(\mathbf{r}) + Q(\mathbf{r}) + Q_{rad}(\mathbf{r}), \tag{2}$$

where $T(\mathbf{r})$ is the temperature, $\rho(\mathbf{r})$ is the mass density, $c(\mathbf{r})$ is specific heat. $\nabla\kappa(\mathbf{r})\nabla T(\mathbf{r})$ represents the conductive heat flux, and $Q_{rad}(\mathbf{r})$ is the radiative heat flux described by Eq. (3) [32],

$$Q_{rad}(\mathbf{r}) = \varepsilon\sigma A(T(\mathbf{r}) - T_{surr})^4, \tag{3}$$

Optics EXPRESS

where $\kappa(\mathbf{r})$ is the thermal conductivity, ε is the emissivity, σ is the Stefan–Boltzmann constant, A is the area of the absorber, $T(\mathbf{r})$ is the surface temperature, and T_{surr} is the surrounding temperature. We used the 'Surface-to-Surface Radiation' interface in the COMSOL heat transfer module to simulate the local heat generated at the MPA while considering both the conductive and radiative heat fluxes [33,34]. This consideration takes into account the radiative cooling effect on the MPA. In contrast, a convective heat flux does not appear in Eq. (2), since exposing the MPA to an infinite-size blackbody radiator considerably minimizes the contribution of the convective heat flux. We defined the surface emissivity of the MPA as equivalent to its reflectivity at each wavelength, i.e., the surface emissivity has wavelength dependence. $Q(\mathbf{r})$ and $T(\mathbf{r})$ were initially calculated for each wavelength at 1 sec (in heat equilibrium). Subsequently, the local heat temperature was obtained by integrating $Q(\mathbf{r})$ and $T(\mathbf{r})$ between 2 and 10 μm. For the simulations, the temperature was probed at the Ag film in the MPA. Govorov et al. reported that the increase in plasmonic local heating of periodic plasmonic nanoparticles cannot be estimated by considering the nanoparticles individually [35,36]. They demonstrated that a temperature increase originating from a two-dimensional array of 16 gold nanoparticles was enhanced more than four times with respect to that of a single nanoparticle; the heating effect can be enhanced by the accumulation effects. Therefore, we calculated the local heating temperatures produced upon changing the number of units of MPAs from 1 to 25 (1×1, 2×2, 3×3, 4×4, and 5×5 units). As the number of units increases, the amount of local heating increases owning to a rise in the external temperature generated by the neighboring MPAs [6,37,38].

Figure 5 shows the logarithmic fits of the plasmonic local temperature versus the number of MPA and control units in the array. The fitted data curves are expressed analytically by Eq. (4) and (5).

$$y = 0.0243 \ln(x) + 0.0615, \tag{4}$$

$$y = 0.0016 \ln(x) + 0.0018, \tag{5}$$

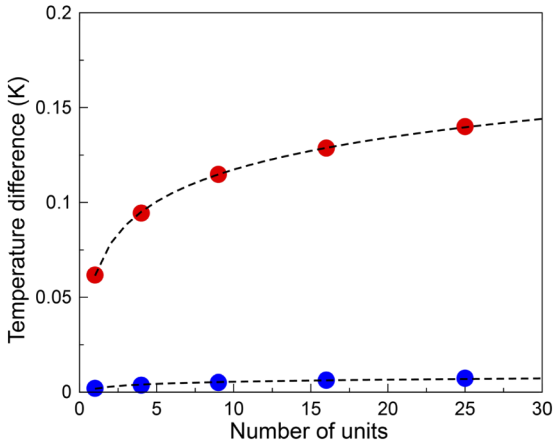

Fig. 5. Dependence of plasmonic local heating on the number of the units in an array. Calculated local heating temperatures as a function of the number of metamaterial perfect absorbers (red circle) and control (blue) units. The dashed lines indicate logarithmic fits to the data.

Since the number of MPAs included in a unit area is 2.5×10^7, the estimated local temperature at the illumination spot is 0.48 K using Eq. (4). There are two reasons for the dominant local heating effect and the minor radiative cooling effect in our calculations. First, the resonance wavelength of our MPA is out of the atmospheric window (8–13 μm) [39]. Second, the radiative

Optics EXPRESS

heat flux Q_{rad} decreases because of the energy that is conserved between the MPA and the surrounding air.

Similarly, we calculated the local heat amount generated on a control device. The control device consists of the bare Bi_2Te_3 with a 100 nm-thick-Ag layer as an electrode on the top. The estimated local temperature at the illumination spot for the control was 0.029 K, calculated using Eq. (5); this is less than 10% that of the MPA. This result indicates that the MPA-Bi_2Te_3 device provides effective additional heat that can improve the thermoelectric performance.

We conducted a heat transfer simulation to study the transfer of the local heat generated at the MPA to the Bi_2Te_3 thermoelectric device. Figure 6(a) shows the plasmonic local heat generation as a function of time calculated for the Ag film with (1×1) MPA unit and at a wavelength of 6.08 μm. The initial temperature of the device and the atmosphere was 500.15 K. An additional heat of 0.045 K was generated on the MPA at 6.08 μm, which was saturated within 2 ms. Figure 6(b) illustrates the heat distribution map of the (1×1) MPA unit calculated at 2 ms, which indicates that the local heating generated at the MPA propagated to the Bi_2Te_3 side mainly by conductive heat propagation. Further, the Ag film served as a suitable thermal conductor to facilitate the local heating propagation to the Bi_2Te_3.

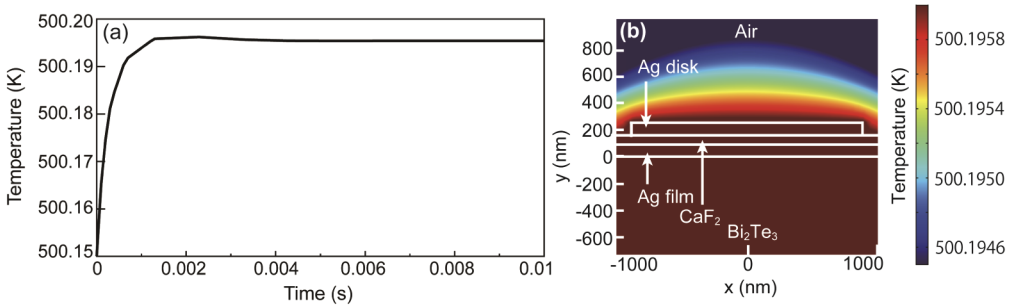

Fig. 6. Time dependence of the plasmonic local heating distributions. (a) The local heat profile as a function of time, calculated at 6.08 μm. (b) X-Z heat distribution map of the metamaterial perfect absorber thermoelectric device with a (1×1) unit, calculated at 2 ms.

3.3. Output power of the thermoelectric device with MPA

The output power calculation for the thermoelectric device was carried out using the COMSOL thermoelectric simulation. The electrical conductivity, thermal conductivity, heat capacity, density, and Seebeck coefficient of Bi_2Te_3 used in the simulation were 1.1×10^5 S/m, 1.636 W/m·K, 154 J/kg·K, 7.7×10^3 kg/m^3, and 210 μV/K, respectively [40]. The thermoelectric simulation revealed that the potential difference between the Cu and the Ag film electrodes was 99.8 μV for the MPA-Bi_2Te_3 thermoelectric device, which was 16 times higher than that generated at a control device. The output power density of the device, calculated by considering the Seebeck coefficient, electrical conductivity, and thermal conductivity of Bi_2Te_3, was found to be 1.09 mW/cm^2 at maximum. The Bi_2Te_3 thermoelectric device was loaded with MPAs that generated an additional output power density that was larger than that of a non-MPA reference device by 1.09 mW/cm^2; this power level is sufficient to drive a wrist watch [41].

Figure 1(b) shows the schematic of the full device that consists of integrated MPA-Bi_2Te_3 thermoelectric devices on a thin substrate. Considering the fabrication accuracy, we assume that each Bi_2Te_3 thermoelectric device is separated from its neighbors by 1-mm and 2-mm spaces to avoid a short circuit. This design involves 7470 units of the thermoelectric devices in one square meter. Thus, the output power density of the integrated MPA-Bi_2Te_3 thermoelectric device is 0.83 W/m^2, which is much higher than the value generated by a flexible thermoelectric

Optics EXPRESS

film exposed to a temperature difference of approximately 70 °C (343 K) [42]. That is, our MPA-Bi_2Te_3 thermoelectric device generates a more output power from solely absorbing thermal radiation at 500.15 K.

4. Conclusion

We proposed an MPA to increase the temperature difference of the thermal gradient across a Bi_2Te_3 thermoelectric device by inducing local heating through the radiation emitted from a heat source at 500.15 K. The MPA with 1.75-μm-diameter and 2-μm-periodicity Ag disks, and a 60-nm-thick CaF_2 layer showed a strong absorption peak at 6.08 μm, close to the peak wavelength of the blackbody radiation spectrum at 500.15 K. Magnetic and electric field distributions calculated at 6.08 μm indicated that this strong absorption is attributed to the magnetic resonance mode of the MPA. Further, electric field confinements that are local heating sites were observed at the edges of the Ag disk. To estimate the local heating, we conducted heat transfer simulations with considerations of absorption and radiation. The experimentally and numerically calculated temperatures in Ref. [37], which reported on the plasmonic local heat temperature generated on silver nanorod array calculated using the same technique as in the present study, were consistent. Therefore, we consider that the numerical results of the present study can be reproduced experimentally. The simulations revealed that when the device surface of the MPA arrays was faced to the infinite-size blackbody radiator at 500.15 K, the MPA arrays generated plasmonic local heating equivalent to 0.48 K. Furthermore, the local heat generated at the MPA propagates to the Bi_2Te_3 within 2 ms. Finally, the local heat of 0.48 K/cm^2 is transferred to the hot side of the Bi_2Te_3 thermoelectric device, leading to an additional thermal gradient across the device. According to the thermoelectric simulations, the Bi_2Te_3 thermoelectric device loaded with the MPA arrays generates an additional output power density of 0.83 W/m^2 compared to that of a reference device without MPAs. However, the effect of the MPA on the Bi_2Te_3 thermoelectric device at different temperatures should be investigated in the future, since the wavelength range and intensity of the thermal radiation spectrum depends on the environmental temperature. Furthermore, the current MPA is not a perfect absorber as it only partially absorbs thermal radiation. Metamaterial arrays with size variations [43] and hyperbolic metamaterials [39,44] can be incorporated in the design of a broadband absorber, which will further improve its output power. The MPA is much thinner than the thermoelectric device; hence, the thermoelectric device loaded with the MPAs can be applied to thin-film thermoelectric devices by appropriately designing the configuration of thermoelectric devices. The simulations and results obtained in the present study pave the way for novel applications of metamaterials as an energy converter of waste heat into electricity.

Funding. Japan Society for the Promotion of Science (Core-to-Core Program, KAKENHI JP-20K05261, JP-18H03889); Core Research for Evolutional Science and Technology (JPMJCR1904); Sumitomo Foundation (191029).

Acknowledgements. W. Kubo thanks the Sumitomo Foundation (191029), the JSPS KAKENHI Grant number JP-20K05261, and the JSPS Core-to-Core Program. The authors acknowledge financial support from JST CREST Grant Number JPMJCR1904 and KAKENHI JP-18H03889, Japan.

Disclosures. The authors declare no conflicts of interest.

References

1. R. Fitriani, B. D. Ovik, M. C. Long, M. Barma, M. F. M. Riaz, S. M. Sabri, R. Said, and Saidur, "A review on nanostructures of high-temperature thermoelectric materials for waste heat recovery," Renewable Sustainable Energy Rev. **64**, 635–659 (2016).
2. A. Fabián-Mijangos, G. Min, and J. Alvarez-Quintana, "Enhanced performance thermoelectric module having asymmetrical legs," Energy Convers. Manage. **148**, 1372–1381 (2017).
3. Z. J. Coppens, W. Li, D. G. Walker, and J. G. Valentine, "Probing and Controlling Photothermal Heat Generation in Plasmonic Nanostructures," Nano Lett. **13**(3), 1023–1028 (2013).
4. M. L. Brongersma, N. J. Halas, and P. Nordlander, "Plasmon-induced hot carrier science and technology," Nat. Nanotechnol. **10**(1), 25–34 (2015).

Optics EXPRESS

5. W. Kubo, M. Kondo, and K. Miwa, "Quantitative Analysis of the Plasmonic Photo-Thermoelectric Phenomenon," J. Phys. Chem. C **123**(35), 21670–21675 (2019).
6. K. Miwa, H. Ebihara, X. Fang, and W. Kubo, "Photo-Thermoelectric Conversion of Plasmonic Nanohole Array," Appl. Sci. **10**(8), 2681 (2020).
7. W. Li and J. Valentine, "Metamaterial Perfect Absorber Based Hot Electron Photodetection," Nano Lett. **14**(6), 3510–3514 (2014).
8. L. R. Hirsch, R. J. Stafford, J. A. Bankson, S. R. Sershen, B. Rivera, R. E. Price, J. D. Hazle, N. J. Halas, and J. L. West, "Nanoshell-mediated near-infrared thermal therapy of tumors under magnetic resonance guidance," Proc. Natl. Acad. Sci. **100**(23), 13549–13554 (2003).
9. X. Huang and M. A. El-Sayed, "Plasmonic photo-thermal therapy (PPTT)," Alexandria J. Med. **47**(1), 1–9 (2011).
10. L. Cao, D. N. Barsic, A. R. Guichard, and M. L. Brongersma, "Plasmon-Assisted Local Temperature Control to Pattern Individual Semiconductor Nanowires and Carbon Nanotubes," Nano Lett. **7**(11), 3523–3527 (2007).
11. S. Ishii, R. P. Sugavaneshwar, and T. Nagao, "Titanium Nitride Nanoparticles as Plasmonic Solar Heat Transducers," J. Phys. Chem. C **120**(4), 2343–2348 (2016).
12. K. W. Mauser, S. Kim, S. Mitrovic, D. Fleischman, R. Pala, K. C. Schwab, and H. A. Atwater, "Resonant thermoelectric nanophotonics," Nat. Nanotechnol. **12**(8), 770–775 (2017).
13. J. W. Stewart, J. H. Vella, W. Li, S. Fan, and M. H. Mikkelsen, "Ultrafast pyroelectric photodetection with on-chip spectral filters," Nat. Mater. **19**(2), 158–162 (2020).
14. A. Safaei, S. Chandra, M. W. Shabbir, M. N. Leuenberger, and D. Chanda, "Dirac plasmon-assisted asymmetric hot carrier generation for room-temperature infrared detection," Nat. Commun. **10**(1), 3498 (2019).
15. V. Shautsova, T. Sidiropoulos, X. Xiao, N. A. Güsken, N. C. G. Black, A. M. Gilbertson, V. Giannini, S. A. Maier, L. F. Cohen, and R. F. Oulton, "Plasmon induced thermoelectric effect in graphene," Nat. Commun. **9**(1), 5190 (2018).
16. C. Wan, Y. Wang, N. Wang, W. Norimatsu, M. Kusunoki, and K. Koumoto, "Development of novel thermoelectric materials by reduction of lattice thermal conductivity," Sci. Technol. Adv. Mater. **11**(4), 044306 (2010).
17. K. Cicvarić, L. Meng, D. W. Newbrook, R. Huang, S. Ye, W. Zhang, A. L. Hector, G. Reid, P. N. Bartlett, and C. H. K. de Groot, "Thermoelectric Properties of Bismuth Telluride Thin Films Electrodeposited from a Nonaqueous Solution," ACS Omega **5**(24), 14679–14688 (2020).
18. A. Moreau, C. Ciracì, J. J. Mock, R. T. Hill, Q. Wang, B. J. Wiley, A. Chilkoti, and D. R. Smith, "Controlled-reflectance surfaces with film-coupled colloidal nanoantennas," Nature **492**(7427), 86–89 (2012).
19. J. Hao, J. Wang, X. Liu, W. J. Padilla, L. Zhou, and M. Qiu, "High performance optical absorber based on a plasmonic metamaterial," Appl. Phys. Lett. **96**(25), 251104 (2010).
20. Z. Y. Xu, R. Z. Wang, and C. Yang, "Perspectives for low-temperature waste heat recovery," Energy **176**, 1037–1043 (2019).
21. C. Forman, I. K. Muritala, R. Pardemann, and B. Meyer, "Estimating the global waste heat potential," Renewable Sustainable Energy Rev. **57**, 1568–1579 (2016).
22. A. Christ, G. Lévéque, O. J. F. Martin, T. Zentgraf, J. Kuhl, C. Bauer, H. Giessen, and S. G. Tikhodeev, "Near-field–induced tunability of surface plasmon polaritons in composite metallic nanostructures," J. Microsc. **229**(2), 344–353 (2008).
23. N. J. Hogan, A. S. Urban, C. Ayala-Orozco, A. Pimpinelli, P. Nordlander, and N. J. Halas, "Nanoparticles Heat through Light Localization," Nano Lett. **14**(8), 4640–4645 (2014).
24. S. V. Boriskina, H. Ghasemi, and G. Chen, "Plasmonic materials for energy: From physics to applications," Mater. Today **16**(10), 375–386 (2013).
25. G. Baffou, R. Quidant, and C. Girard, "Heat generation in plasmonic nanostructures: Influence of morphology," Appl. Phys. Lett. **94**(15), 153109 (2009).
26. G. Baffou and R. Quidant, "Thermo-plasmonics: using metallic nanostructures as nano-sources of heat," Laser Photonics Rev. **7**(2), 171–187 (2013).
27. S. Katsumata, T. Isegawa, T. Okamoto, and W. Kubo, "Effect of Metamaterial Perfect Absorber on Device Performance of PCPDTBT:PC71BM Solar Cell," Phys. Status Solidi A **217**(1), 1900910 (2020).
28. T. Isegawa, T. Okamoto, M. Kondo, S. Katsumata, and W. Kubo, "P3HT:PC61BM solar cell embedding silver nanostripes for light absorption enhancement," Opt. Commun. **441**, 21–25 (2019).
29. N. I. Landy, S. Sajuyigbe, J. J. Mock, D. R. Smith, and W. J. Padilla, "Perfect Metamaterial Absorber," Phys. Rev. Lett. **100**(20), 207402 (2008).
30. H. H. Richardson, M. T. Carlson, P. J. Tandler, P. Hernandez, and A. O. Govorov, "Experimental and Theoretical Studies of Light-to-Heat Conversion and Collective Heating Effects in Metal Nanoparticle Solutions," Nano Lett. **9**(3), 1139–1146 (2009).
31. G. Baffou and H. Rigneault, "Femtosecond-pulsed optical heating of gold nanoparticles," Phys. Rev. B **84**(3), 035415 (2011).
32. X. Zhao, X.-J. Zha, J.-H. Pu, L. Bai, R.-Y. Bao, Z.-Y. Liu, M.-B. Yang, and W. Yang, "Macroporous three-dimensional MXene architectures for highly efficient solar steam generation," J. Mater. Chem. A **7**(17), 10446–10455 (2019).
33. R. Van Eck, M. Klep, and J. Schijndel, "Surface to Surface Radiation Benchmarks," presented at the *Comsol Conference, Munich, Germany* 2016.
34. X. Liu, T. Tyler, T. Starr, A. F. Starr, N. M. Jokerst, and W. J. Padilla, "Taming the Blackbody with Infrared Metamaterials as Selective Thermal Emitters," Phys. Rev. Lett. **107**(4), 045901 (2011).

Optics EXPRESS

35. A. O. Govorov, W. Zhang, T. Skeini, H. Richardson, J. Lee, and N. A. Kotov, "Gold nanoparticle ensembles as heaters and actuators: melting and collective plasmon resonances," Nanoscale Res. Lett. **1**(1), 84–90 (2006).
36. A. O. Govorov and H. H. Richardson, "Generating heat with metal nanoparticles," Nano Today **2**(1), 30–38 (2007).
37. G. Baffou, P. Berto, E. Bermúdez Ureña, R. Quidant, S. Monneret, J. Polleux, and H. Rigneault, "Photoinduced Heating of Nanoparticle Arrays," ACS Nano **7**(8), 6478–6488 (2013).
38. G. Baffou, P. Bon, J. Savatier, J. Polleux, M. Zhu, M. Merlin, H. Rigneault, and S. Monneret, "Thermal Imaging of Nanostructures by Quantitative Optical Phase Analysis," ACS Nano **6**(3), 2452–2458 (2012).
39. M. M. Hossain, B. Jia, and M. Gu, "Metamaterials: A Metamaterial Emitter for Highly Efficient Radiative Cooling," Adv. Opt. Mater. **3**(8), 1047–1051 (2015).
40. E. E. Antonova and D. C. Looman, "Finite elements for thermoelectric device analysis in ANSYS," in *ICT 2005. 24th International Conference on Thermoelectrics, 2005.*(2005), pp. 215–218.
41. M. A. Zoui, S. Bentouba, J. G. Stocholm, and M. Bourouis, "A Review on Thermoelectric Generators: Progress and Applications," Energies **13**(14), 3606 (2020).
42. K. Suemori, S. Hoshino, and T. Kamata, "Flexible and lightweight thermoelectric generators composed of carbon nanotube–polystyrene composites printed on film substrate," Appl. Phys. Lett. **103**(15), 153902 (2013).
43. A. K. Azad, W. J. M. Kort-Kamp, M. Sykora, N. R. Weisse-Bernstein, T. S. Luk, A. J. Taylor, D. A. R. Dalvit, and H.-T. Chen, "Metasurface Broadband Solar Absorber," Sci. Rep. **6**(1), 20347 (2016).
44. Z. Wang, P. Yang, G. Qi, Z. M. Zhang, and P. Cheng, "An experimental study of a nearly perfect absorber made from a natural hyperbolic material for harvesting solar energy," J. Appl. Phys. **127**(23), 233102 (2020).